Adsorption sites on icosahedral quasicrystal surfaces: dark stars and white flowers

2009 J. Phys.: Condens. Matter 21 055009

(http://iopscience.iop.org/0953-8984/21/5/055009)

J. Phys.: Condens. Matter **21** (2009) 055009 (10pp) doi:10.1088/0953-8984/21/5/055009

Adsorption sites on icosahedral quasicrystal surfaces: dark stars and white flowers

Barış Ünal[1,2], **C J Jenks**[2] **and P A Thiel**[1,2,3]

[1] Department of Materials Science and Engineering, Iowa State University, Ames, IA 50011, USA
[2] Ames Laboratory, Ames, IA 50011, USA
[3] Department of Chemistry, Iowa State University, Ames, IA 50011, USA

E-mail: thiel@ameslab.gov

Received 29 October 2008, in final form 15 December 2008
Published 12 January 2009
Online at stacks.iop.org/JPhysCM/21/055009

Abstract

From other work, two preferred sites have been suggested for metals and semimetals adsorbed on the fivefold surfaces of icosahedral, Al-based quasicrystals. Because of their appearance in scanning tunneling microscopy (STM) images, these sites are known as dark stars and white flowers. In this paper, we analyze four bulk structural models in physical space to determine the types, chemical decorations, and densities of the dark star—and, to a lesser extent, the white flower—adsorption sites for the fivefold planes of icosahedral Al–Pd–Mn. We find that the chemical decorations of these sites are heterogeneous, even within a single model. Both features are also structurally heterogeneous, according to STM measurements, and the structural variation is consistent with the bulk structure models. Finally, from the models, the density of dark stars in the planes correlates with the step height. This may explain previous experimental observations of different properties for different terraces.

(Some figures in this article are in colour only in the electronic version)

1. Introduction

The surface adsorption site of a molecule or an atom is one of the most basic facts that is needed to understand chemisorption. However, extracting this simple information poses special challenges when studying chemisorption on a type of intermetallic alloy known as a quasicrystal. These challenges ultimately derive from the fact that quasicrystals are well-ordered, but are not periodic. A direct consequence for surface science is that quasicrystals naturally present multiple types of adsorption sites, where a site is defined as a local minimum in the potential energy surface. A good illustration of the variety expected for a quasicrystal is shown in figure 2 of [1], which is a potential energy surface calculated for an Al adatom on fivefold i-Al–Cu–Fe. The range of adsorption sites is due to the range of local atomic configurations that can be identified.

A particular type of quasicrystal—the icosahedral (i-), Al-based alloy—has received much attention from surface scientists, because materials in this class are available as large single-grain samples, because they are tractable in ultrahigh vacuum (UHV), and because they represent a large fraction of known quasicrystals. This paper focuses upon i-Al–Pd–Mn, although some mention is made of two alloys believed to be isostructural, i-Al–Cu–Ru and i-Al–Cu–Fe. The fivefold surfaces of these alloys are believed to be bulk-terminated, except for interplanar relaxation [2–8].

Experimental work has shown that two particular adsorption sites are preferred [9]. The preferred site depends on the adsorbate. For Al, Ag, Sn and C_{60} adsorbates [9–14], the preferred site is imaged as a dark star in scanning tunneling microscopy (STM) of the clean fivefold surfaces of i-Al–Pd–Mn and i-Al–Cu–Fe [10, 11]. In nucleation and growth of Ag films, this site acts as a 'trap' site, skewing the nucleation kinetics to resemble heterogeneous nucleation [13, 15]. For adsorbed Bi [16] and Si [17], the preferred site is imaged as a white flower in STM of the same surfaces. While the nucleation kinetics has not been studied in the latter system, one expects a trapping effect to be exhibited by the white flowers as well.

In this paper, we explore the possible chemical and structural nature of the dark star site and, to a lesser extent, of the white flower site. The spectrum of possibilities for these sites is much more complex than in a normal crystal. The complicating factors include the existence of different models for the bulk structure; the existence of different possible families of terminations within any given model; and the possibility of sites that are structurally identical but chemically different, even within a single family of a single model. This work builds upon a previous report, in which we analyzed the variation in the long-range, average density and composition of surface terminations for different models of the bulk structure and for different families of terminations [18]. The present work is different because it focuses on a *local* feature—the adsorption site.

Some other publications have analyzed aspects of dark star and white flower sites (and other motifs) [19–21] for a single model, but there has been no comparison among different models such as that presented here. Thus, while this paper overlaps somewhat with publications from other groups, it presents many new pieces of information—both from experiment and from analysis of the models—that contribute to a more comprehensive and useful picture. For instance, by pointing out the variability in chemical decoration of dark star sites among different models, or among different terminations, one gains insight into the robustness of theoretical analyses of adsorption on quasicrystal surfaces.

This paper also analyzes the densities of the dark star sites. One interesting result is that the density should correlate with the height of the step that borders the terrace based on the bulk models, which might explain some experimental observations showing that different quasicrystal terraces can behave differently in adsorption [22, 23]. Finally, we present new experimental data that support the existence of different types of dark star sites on real terraces.

2. Background

2.1. Families of terminations

Bulk structure models of quasicrystals are often called 'deterministic' if they contain no sites of partial or mixed occupancy. In this paper, we focus on four deterministic bulk structure models, and comment briefly about one non-deterministic model. These five models are chosen because they have been made available in the form of large three-dimensional volumes containing atomic coordinates. We refer to them as the Boudard model, the Katz–Gratias (KG) model, the Quiquandon–Gratias (QG) model, and the Papadopolos–Kasner (PK) model. Details of our approach have been given previously [18].

It is known that surfaces of quasicrystals can be prepared in a terrace-step structure, in which the terraces are essentially flat [7, 24–28]. Therefore, it is useful to break down the bulk models into atomic planes, for purposes of comparison with surfaces. Figure 1 shows an example of the density and composition of planes of atoms, versus their location along the fivefold axis in one of the deterministic models (PK). If we ignore the low-density planes (lower than about 1 atom nm^{-2}), the four deterministic models are virtually identical when represented in the style of figure 1 [18]. This is not surprising; it has been said that about 85% of the atomic sites overlap in these models, a fact which derives from certain common features in their six-dimensional structure [18, 29].

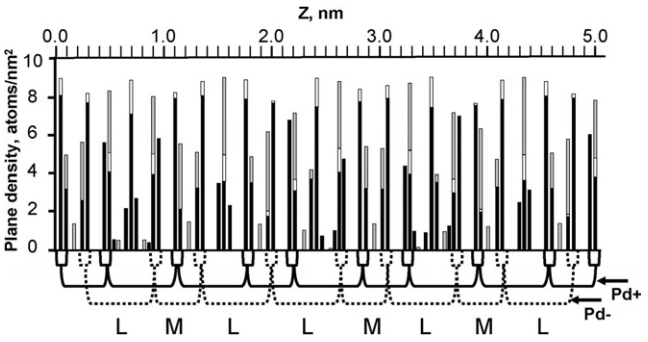

Figure 1. Schematic depiction of atomic planes in the PK model. The z-axis is the fivefold axis. The spatial coordinate is labeled '(z)' because this is the notation used by the authors of the model. The height of each line is proportional to the planar atomic density. Within each vertical bar, black is Al, gray is Pd, and white is Mn.

Several experiments have shown that the preferred terminations of fivefold surfaces of i-Al–Pd–Mn and i-Al–Cu–Fe consist of two dense planes that are closely spaced. The spacing between the planes at the surface is about 0.04 nm, a contraction of 20% from the bulk value of 0.05 nm [2–5]. We shall call such a pair of planes a *layer*. Furthermore, experiments show that terraces are separated by steps of various heights, where the heights are related by the golden mean, $\tau = (1 + \sqrt{5})/2 \approx 1.618$ [7, 24–28, 30].

Matching these two features to the models, we identified two main families of layers as viable terminations [18]. Some are labeled at the bottom of figure 1 with brackets. In one family, the top plane contains Pd, and in the other it does not. Hence, we call them Pd− (without Pd) and Pd+ (with Pd). Besides Pd content, these two families differ in the average relative densities of the two planes (Pd− having the denser plane on top, usually) and the width of the interplanar gap where the surface forms (Pd− having the larger gap by a factor of 2). A third family is also present but as a minority. Based upon comparison with experimental data, and upon the widths of the gaps in the models, we concluded that the Pd− family is most likely to be the favored type of termination [18].

2.2. Clusters in the bulk models

The analysis of the dark star and white flower sites is typically couched in terms of clusters that can be identified in the bulk solid. When a surface plane intersects a cluster, the cluster is truncated (cut). In the bulk, the clusters contain a few tens of atoms arranged in concentric shells. In the deterministic models, the two main types of clusters are called Mackay and Bergman.

The Bergman cluster is a two-shell cluster. The central site can be filled with a single atom, or empty. The inner shell is an icosahedron (12 vertices), and the outer is a dodecahedron

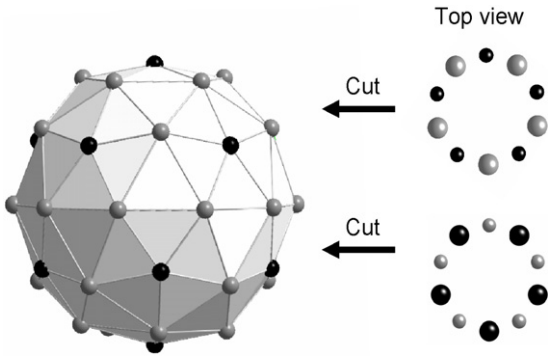

Figure 2. A Mackay cluster. Black spheres are the vertices of the icosahedron and gray spheres are the vertices of the icosidodecahedron. Cuts show ways of forming pentagonal hollows.

(20 vertices) with diameter 0.83 nm. If all sites are filled and the structure is geometrically ideal, the number of atoms in a Bergman cluster is 33.

The Mackay cluster, shown in figure 2, has three shells and 50 atoms on average, including a central atom. In this cluster, the inner polyhedron is an incomplete dodecahedron, sometimes termed a disordered dodecahedron because the number and positions of atoms vary from cluster to cluster. This incomplete dodecahedron is enclosed by two interpenetrating polyhedra containing (ideally) 42 atoms: a complete icosahedron (12 vertices), plus a complete icosidodecahedron (30 vertices). The diameters of the last two shells are both 0.96 nm. (Note that here we are defining the terms 'Bergman cluster' and 'Mackay cluster' in a way that is consistent with current discussions of quasicrystals. In the *original* definitions given by Bergman *et al* [31] and by Mackay [32], both clusters had more, larger shells. The clusters discussed in this paper are thus geometrical subsets of the original clusters.)

In Al–Pd–Mn quasicrystals, Mackay and Bergman clusters are not independent, because they often overlap. The overlap is illustrated, for instance, by figure 10 of [33]. Because of overlap, the clusters are almost space-filling. In the QG model, for example, they fill 98% of the volume of the solid [34]. The interpenetration of these clusters leads to variations in structural and chemical order within a given type of cluster.

Many clusters are imperfect. They can deviate from ideality due to missing atoms, extra atoms, and/or distortion. In this vein, an extensive analysis of Mackay clusters in the Boudard model has shown that at least 22% of the Mackay clusters lack one or more atoms in the outer two shells [35]. Further insight into structural variation has been provided by analyses of the KG and QG models [33, 34], showing that the number of atoms in Bergman clusters ranges from 32 to 35, with numbers in excess of 33 indicating distortion. In this paper, surface features are described as cut Bergman (cB) or cut Mackay (cM) clusters if the number and arrangement of atoms *in the first surface layer* (i.e. in the first pair of planes) matches expectation for a truncated cluster of that type, regardless of whether the remainder of the cluster in the bulk is perfect. We believe that this definition of a cut cluster is good for comparison with experimental STM data. However, it may be different than that which has been adopted by other authors, for instance Papadopolos *et al* [36], in their analyses of densities of cBs in surface terminations.

Chemical variations are also common in the bulk, both from cluster to cluster and from model to model. For instance, consider the Mackay clusters. The central atom can be either Al or Mn in the Boudard and KG models. It can be either Al or Pd in the QG model. The icosahedron (one of the two outer shells) can contain Al, Mn, and/or Pd in the Boudard model, but it is either pure Pd or pure Mn in the QG model. The distorted dodecahedron (the innermost shell of the Mackay) is always pure Al in perfect clusters, but it can contain other kinds of atoms in imperfect clusters.

The clusters in the Yamamoto model are larger than those of the other models. For example, there are two main clusters with 2.0 nm diameter. These clusters have 12 and 11 concentric shells, respectively (see figures 10 and 11 in [37]). As in the deterministic models, the chemical decorations of the bulk clusters in this model can vary within limits. For example, in the 12-shell clusters, the vertices of the innermost polyhedron are decorated by Pd and/or Mn, and the vertices of the next polyhedron are decorated by Al and/or Mn. Although these clusters are larger than those in the deterministic models, in both the 12-shell and 11-shell clusters, the first two inner shells are Bergman clusters.

In the Yamamoto model, there are also two types of three-shell Mackay clusters (see figure 12 in [37]). The first has a fully occupied icosahedron as the inner shell, while the second has a partially occupied dodecahedron. The chemical decorations of both clusters can vary.

In summary, the clusters in the Yamamoto model are similar to those in the deterministic models, if one considers only the inner shells. Our further analysis is restricted to the deterministic models, because the Yamamoto model is relatively complex and heterogeneous.

3. Results and discussion

3.1. Experimental surface data

A high resolution STM image of the fivefold surface of i-Al–Pd–Mn is shown in figure 3. There, examples of dark stars and white flowers are marked, as well as two other motifs known as white stars and rings. Previously, other groups also observed these local atomic configurations with STM [20, 24, 25, 27, 36, 38]. Among all of the local structures, dark stars and white flowers are the most abundant motifs. The following observations can be made about these two features.

(i) All dark stars in figure 3(a) have the same size and shape, but a close inspection reveals that there are at least three types of local environments in the STM image. Each dark star is surrounded by five, four or fewer than four complete pentagons. Based on this, we classify the dark stars as A-, B- and C-type, respectively. These types are marked in the STM image of figure 3(a), and are also drawn schematically in figure 3(b). Whenever a pentagon is missing between two arms of a dark star, a single protrusion stands in its place.

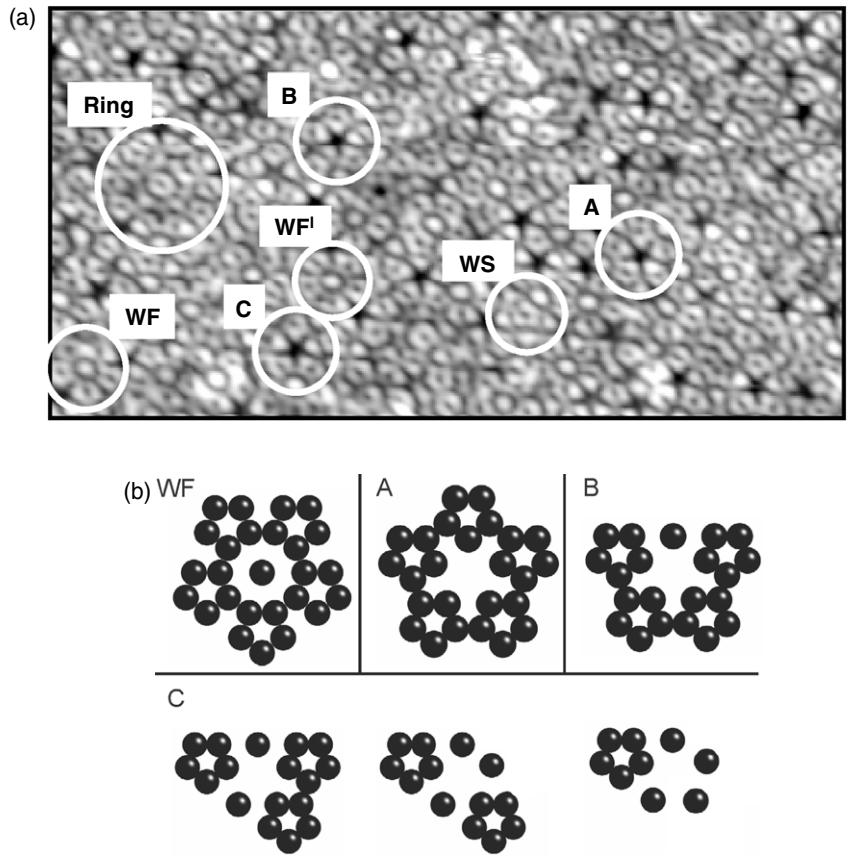

Figure 3. (a) An *unfiltered* STM image of a clean fivefold surface of i-Al–Pd–Mn quasicrystal. The tunneling conditions: 0.47 nA and +0.97 V. Size of the image is 25.1 × 12.1 nm^2. Letters A, B, and C denote the three types of dark stars. Two types of white flowers are marked as WF (complete) and WF′ (incomplete). A ring motif and a white star (WS) are also marked. (b) Schematic depiction of three different kinds of dark stars and a complete white flower, as observed in STM. Note that an incomplete dark star, like B or C, is distinguished not only by the local appearance of its arms, but also by its overlap with a white star (WS). In other words, the corner of a WS replaces one (or more) of the pentagonal arms of the incomplete dark stars.

(ii) The depth of the dark stars varies within the same terrace. This is illustrated by the line profiles in figure 4, which cut across three dark star sites. One is significantly deeper than the other two.

(iii) The orientation of the dark stars is the same within a single terrace as shown in figure 3(a). The orientation is also the same across different terraces. This is not shown here, but see figure 3 in [39] and figure 4 in [38].

(iv) The density of dark stars changes from terrace to terrace. This is not shown here, but see figure 3 in [39], figure 4 in [38], or figure 2 in [40] for examples.

(v) As shown by comparing figure 4(a) with (b), there is some dependence upon whether the image is raw or filtered. The apparent density of dark stars increases with fast Fourier transformation (FFT) filtering, because filtering converts some poorly-imaged features into dark stars. Examples are encircled in figures 4(a) and (b). On the other hand, the conclusion that dark stars have different depths is not affected by filtering. Also, once a dark star has been identified, its classification as A-, B-, or C-type does not depend upon filtering.

(vi) An ideal white flower is formed by five small pentagons centered on a single small protrusion, but most of the white flowers are not perfect. This is because, in a typical white flower, one or more of the pentagons appear incomplete as shown in figure 3(a).

3.2. *Surface structure from the bulk models*

3.2.1. Positions of atoms. Previously, Papadopolos *et al* carried out an extensive analysis, showing that the basic motifs seen with STM—dark star, white flower, white star, ring—can be identified in the Pd+ family of terminations within the PK model. Most notably, the dark star site was identified as a cB truncated at 0.076 nm below its equator. In addition, a white flower was described by five intact Bergman clusters hanging down from the surface plane [20, 36]. We have extended the analysis to the other three deterministic models. We find that the same cB configuration can be found in all models, in the Pd+ family. This is not surprising, because of the extensive overlap in atomic positions between models (cf section 2.1). However, as noted in section 2.1, the Pd+ family of terminations is less favored than the Pd− family.

In the Pd− family of terminations, atomic arrangements corresponding to the four experimentally-observed motifs can also be identified, in all four of the deterministic models. Figure 5 shows atomic positions within the top two planes of a Pd− termination from the PK model. Each circle represents

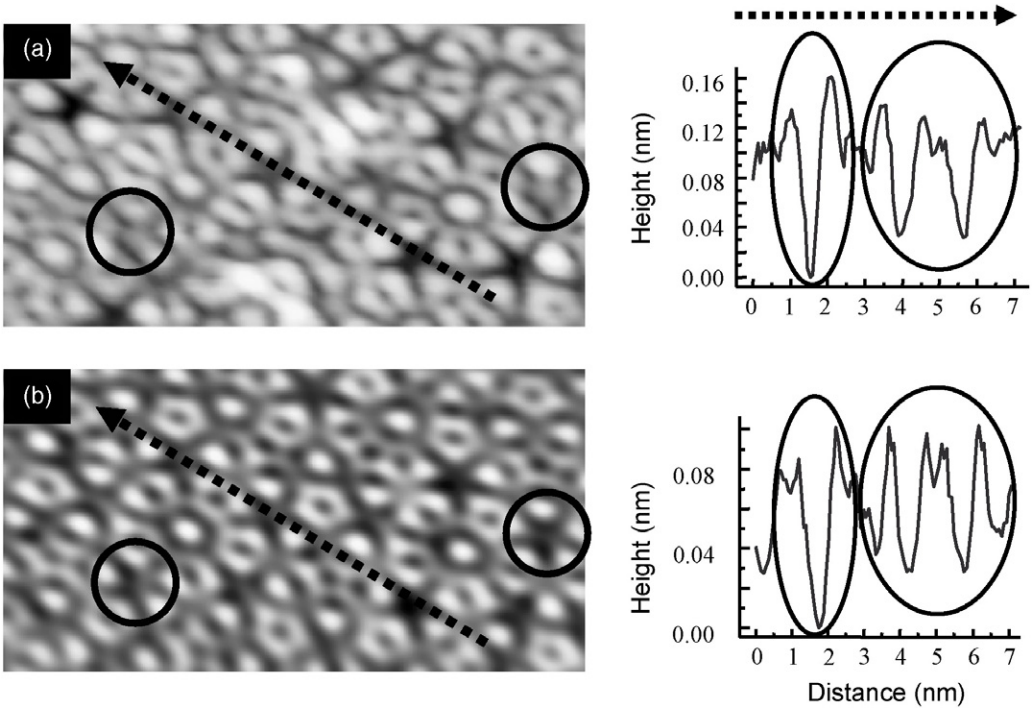

Figure 4. STM images of the clean fivefold surface of i-Al–Pd–Mn quasicrystal. The image size is 8.6 × 4.5 nm^2. (a) Raw data. (b) FFT filtered. Circles show dark stars that appear to have extra atom(s) near the central site. This central material is suppressed, and the dark star character is enhanced, by filtering. The dashed arrows indicate the cut of the line profiles shown at right.

an atom, irrespective of the type of element. As marked in figure 5, a hollow site surrounded by small pentagons is a reasonable candidate for a dark star, and five small pentagons centered on a single atom in the top plane is a good match to a white flower. A small pentagon surrounded by five atoms occupying the vertices of a larger pentagon can be a white star. Ten small pentagons centered on a small pentagon can be a ring motif.

Previously, Krajci *et al* [21], showed that two of these four local features—dark star and white flower—exist in the Pd− family of a 3/2-type approximant. They showed that the geometric arrangement of top-plane atoms translates well into geometric features in STM images, for these two motifs. This was based upon a DFT simulation of STM images for this approximant.

Focusing now on the pentagonal hollow motifs, figure 6(a) demonstrates that not all have the same local structural environment in the models. They are surrounded by either five, four, or less than four complete pentagons, making them analogous to the A-, B-, and C-type dark stars observed experimentally (cf figures 3(a) and (b)). When a perfect pentagon is absent, it is replaced by three atoms in the topmost plane. The innermost of these atoms corresponds well to the single protrusion observed at these locations with STM. Thus, three types of pentagonal hollow sites exist in the models, and these may be the three types of dark stars identified in experiment, based upon local environment.

If a Mackay is cut 0.252 nm above the center atom, as shown by the top arrow in figure 2, a pentagon of atoms with an edge length of 0.48 nm is produced. This gives the main geometry of the dark star [21, 41]. This top pentagon

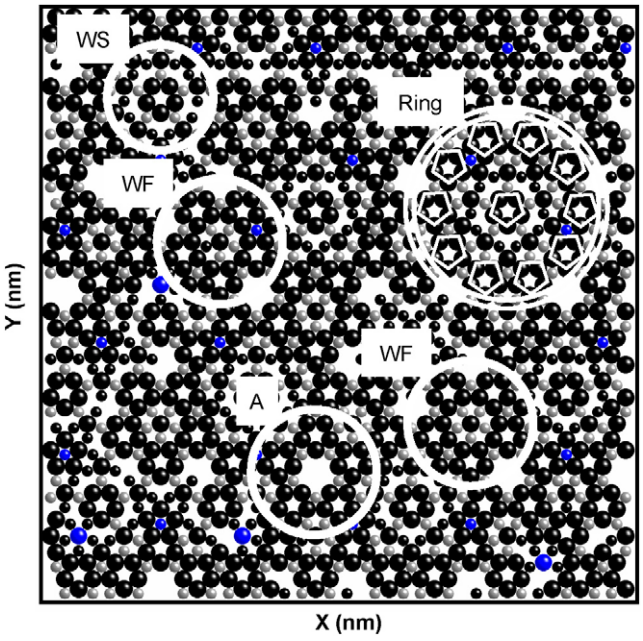

Figure 5. Top view of a layer from the PK model at 2.00 nm. The size of the layer is 10 × 10 nm^2. Each ball represents an atom. Black is Al, blue is Mn and gray is Pd. The circle marks the ring motif. A dark star (A), a white star (WS) and two white flower (WF) motifs are also marked by circles.

arises from atoms in the icosidodecahedral shell. In the plane immediately beneath is another pentagon of atoms, rotated by 36°, arising from the icosahedral shell. In STM, one would expect the vertices of the second pentagon to be aligned with

Table 1. Range of densities of cut Mackay (cM) pentagonal hollow sites in Pd-terminations, from four bulk structure models. In calculating the averages, each plane is weighted according to its area.

	Densities of A-type cM pentagonal hollows (nm^{-2})		Densities of B-type cM pentagonal hollows (nm^{-2})		Densities of C-type cM pentagonal hollows (nm^{-2})		All types of cM pentagonal hollows combined (A + B + C) (nm^{-2})	
Model	Range	Average	Range	Average	Range	Average	Range	Average
Boudard	0–0.170	0.038	0–0.150	0.022	0–0.840	0.190	0–0.840	0.250
KG	0–0.131	0.036	0–0.150	0.024	0–0.833	0.208	0–0.833	0.268
QG	0–0.180	0.038	0–0.130	0.024	0–0.890	0.194	0–0.890	0.257
PK	0–0.160	0.039	0–0.150	0.024	0–0.940	0.183	0–0.940	0.246

Table 2. Densities of pentagonal hollow sites, and of top planes, in specific Pd− terminations in the PK model. For a terrace (plane) at a given position, the height of the descending step is the difference between its position and the position of the terrace (plane) beneath it, i.e. the difference between the two numbers in the far left column.

Position of top plane in the termination, along the fivefold axis (nm)	Descending steps (nm)	Density of A-type cM pentagonal hollows (nm^{-2})	Density of B-type cM pentagonal hollows (nm^{-2})	Density of C-type cM pentagonal hollows (nm^{-2})	Total density of cM pentagonal hollows (nm^{-2})	Atomic density of top plane (nm^{-2})
4.800	0.66	0.160	0.000	0.000	0.160	8.170
4.140	0.41	0.000	0.000	0.000	0.000	8.900
3.730	0.66	0.030	0.050	0.270	0.350	6.980
3.070	0.41	0.060	0.000	0.000	0.060	8.600
2.660	0.66	0.000	0.000	0.810	0.810	4.780
2.000	0.66	0.080	0.150	0.040	0.270	7.710
1.340	0.41	0.000	0.000	0.000	0.000	8.820
0.930	0.66	0.000	0.000	0.610	0.610	5.790
0.270	0.66	0.160	0.000	0.000	0.160	8.180
−0.390	0.41	0.000	0.000	0.000	0.000	8.860
−0.800	0.66	0.040	0.040	0.330	0.410	6.870
−1.460	0.41	0.050	0.000	0.000	0.050	8.640
−1.870	0.66	0.000	0.000	0.940	0.940	4.980
−2.530	0.66	0.090	0.090	0.000	0.180	7.760
−3.190	0.41	0.000	0.000	0.000	0.000	8.850
−3.600	0.66	0.010	0.000	0.530	0.540	6.500
−4.260	—	0.070	0.000	0.000	0.070	8.460

the arms of the dark stars. A similar result can be obtained if a Mackay cluster is cut 0.204 nm below the center (see bottom arrow in figure 2), except now the origins of atoms in the two pentagons are reversed. These, and other aspects of the dark star structure, are shown by figures 2 and 6(b). Note that these two cuts yield identical atomic configurations in the top layer, and would be indistinguishable with STM.

All the pentagonal hollows have the same orientation, both within a given termination and on different terminations, consistent with experimental observation (point (iii) in section 3.1). However, their density changes from termination to termination. A density variation among terraces has also been observed with STM [38–40]. The average value and range of densities of cMs, for each model, are summarized in table 1. One sees that there is almost no difference between the models, because the atomic positions in the dense planes are so similar among the models.

The densities of pentagonal hollows, for a set of individual Pd− terminations in the PK model, are given in table 2. One sees here that the density of pentagonal hollows decreases as the density of atoms in the topmost plane increases; some terminations contain no hollows. This trend is also shown in figure 7. The rationale for this correlation involves the disordered dodecahedron.

Atoms from the disordered dodecahedron (the inner shell) can occupy positions close to the center of a pentagonal hollow in either the second plane, or in the top plane. These two cases are shown in figures 6(b) and (c), respectively. If atoms are in the top plane, they probably prevent cMs from being imaged as dark stars with STM. Therefore, we do not count such configurations as dark stars in our analyses. (In potential energy surface calculations, atoms in these positions cause the pentagonal hollows to have a banana-like appearance [1, 21, 41, 42].) The population of these atoms increases as the atomic density of the top plane increases, hence causing a decrease in dark star density.

Atoms from the disordered dodecahedron can also be in the second plane. For the A-, B-, and C-type dark stars there are 0, 1, and 2 such atoms, respectively. The variable contribution of this inner shell is one possible reason for the different depths of dark stars observed in the STM images. However, the logical consequence would be a correlation between the type and depth of the dark star, which our experimental data do not support. A possible explanation is that the inner dodecahedron is less perfect at the surface than is the surrounding matrix. Specifically, the atoms of the inner dodecahedron could be less strongly-bound and hence dislodged or filled incorrectly during the annealing process by which the surface is formed.

Turning now to the white flower feature, it has three central components, as shown in figure 6(a): a center atom in the top plane, a pentagon of atoms in the second plane, and

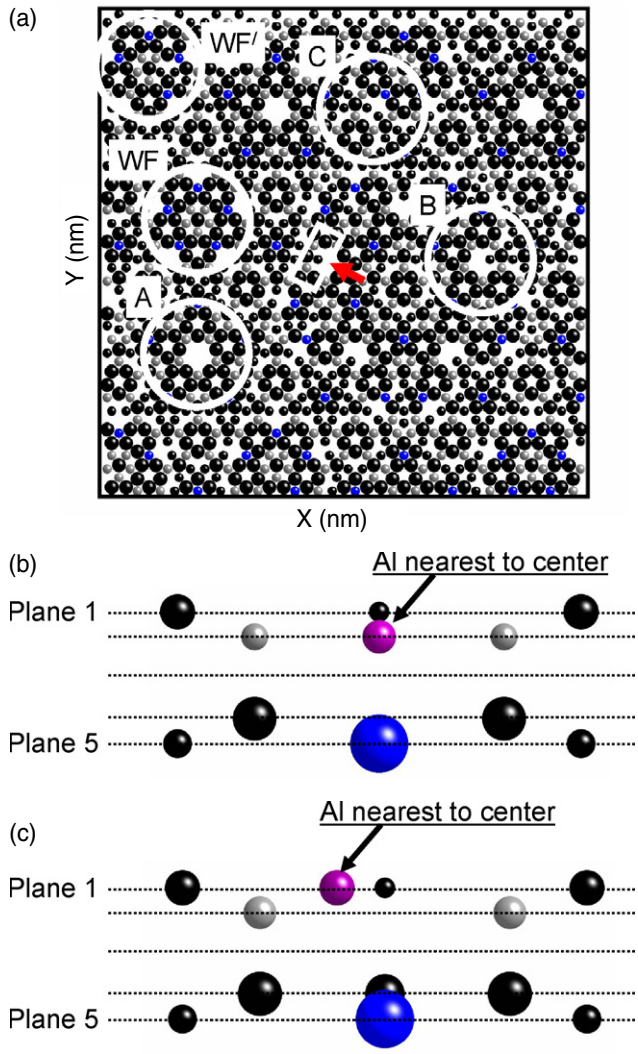

Figure 6. (a) Top view of a layer from the PK model at 3.78 nm. Three types of dark stars—A, B, and C—are marked by circles. Several white flower (WF) motifs are also marked by circles. In the middle region, a white rectangle shows the region of the cross-section in (b). A red arrow shows the view direction. This is a cut across a B-type dark star. It intersects an atom from the disordered inner dodecahedron. ((b), (c)) Cross-sections of cMs, formed by cuts 0.252 nm above their equator. Each ball represents an atom. Black is Al, blue (dark gray in the printed version) is Mn and light gray is Pd. Al atoms (pink) from the inner dodecahedron are labeled. Atoms in the top-plane pentagon are from the icosidodecahedron. Atoms in the second-plane pentagon are from the icosahedron. A central atom (blue) in the cluster is also shown. The size of the balls is related to the position of atoms with respect to the viewer (i.e. closer atoms are drawn larger).

a ten-atom decagon in the top plane. The ten-atom decagon forms the inner edges of five outer pentagons (the 'petals' of the flower) in the top plane. The white flower can be formed in two ways in the Pd− family of terminations. First, a surface plane can cut the Mackay cluster at its equator. Then the five petals of the white flower are formed by five Bergmans cut 0.124 nm above their equator. Here, the atom at the center of the white flower is the center atom of the Mackay cluster. In the second way, the Mackay is tangent to (hanging down from) the surface plane, with five surrounding Bergmans, cut the same

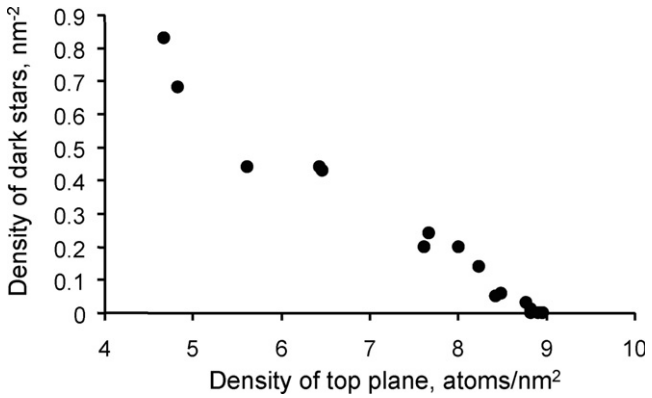

Figure 7. Density of cM pentagonal holes (equated with dark stars), versus densities of top planes, in the PK model.

as before. The center atom belongs to the icosahedron of the Mackay, not its center. Analogous to the dark stars, these two cuts yield identical atomic configurations in the top layer, and would probably be indistinguishable with STM. Previously, the white flower has been identified with only the first of these two configurations, i.e. the Mackay cut at its equator [21].

3.2.2. Identities of atoms. In this analysis, we consider the dark star sites to be cMs for reasons discussed in section 2.1. The chemical decorations of the dark stars, within the top two planes, are shown in table 3. For two of the geometric features that make up the dark star, the chemical decorations are relatively invariant. The first is the pentagon of atoms in the top plane, with edge length 0.48 nm. This is almost always entirely Al. The sole exception is the QG model, where one of the pentagonal vertices is occasionally occupied by Mn. Second, the second-plane atoms that arise from the inner dodecahedron are usually Al, but some C-type dark stars have one or two Pd atoms in the second plane in both QG and KG models.

More chemical variation exists in the pentagon of atoms (with edge length of 0.48 nm) in the second plane, which is rotated by 36° with respect to the top pentagon. This is qualitatively summarized in table 3. In the Boudard model, the atoms at the vertices of the second-plane pentagon can be Mn, Pd, or a mixture of Mn and Pd. In the QG model, they can be Al, Pd, or a mixture of Al and Pd. In the KG and PK models, the pentagons can consist of any of the three elements alone, and in addition some terminations have a mixture of Al, Pd and Mn at these sites. A termination with mixed compositions in some of the second-plane pentagons, from the PK model, is illustrated in figure 6(a). The chemical decoration of the second-plane pentagon varies considerably among models, among terminations within a given model, and among clusters within a given termination of a single model.

The chemical identities of the white flowers are also model-dependent in a complex way, as shown in table 4. Consider first the central components: the center atom, the vertices of the pentagon in the second plane, and the ten-atom decagon in the top plane. In all models, the center atom is either Al or Mn, except for the KG model where the center is always Al. In all models, the ten-atom decagon is decorated by

Table 3. Chemical decorations of A-, B-, and C-type pentagonal hollows from cut Mackays, in the bulk structural models of i-Al–Pd–Mn quasicrystals. The letters in parentheses denote the type of pentagonal hole.

	Model types			
Type of features	Boudard	KG	QG	PK
Pentagon in top plane	Al (A, B, C)	Al (A, B, C)	Al (A, B, C), Mn (A)	Al (A, B, C)
Pentagon in second plane	Pd (A), Mn (A, B, C), Pd + Mn (A, B, C), Al + Pd + Mn (C)	Al (A, B, C), Pd (A), Mn (A, B, C), Al + Mn (B, C), Pd + Mn (C), Al + Pd + Mn (C)	Al (A), Pd (A, B, C), Al + Pd (B, C)	Pd (A, B, C), Al + Mn (C), Pd + Mn (C), Al + Pd + Mn (C)

Table 4. Chemical decorations of white flowers in the bulk structural models of i-Al–Pd–Mn quasicrystals.

	Model types						
Type of features	Boudard		KG	QG		PK	
Center atom	Al	Mn	Al	Al	Mn	Al	Mn
Ten-atom ring in first plane	Al	Al	Al	Al	Al, Al + Mn	Al	Al
Pentagon in second plane	Pd, Al + Pd, Al + Pd + Mn	Al, Al + Pd	Al, Pd, Al + Pd	Al, Pd	Al, Al + Pd	Pd, Al + Pd	Al

Al atoms only, except for the QG model where this decagon is a mixture of Al + Mn if the center is occupied by Mn. As shown in table 4, the second-plane pentagon exhibits more chemical variation. Furthermore, in all models, some of the vertices of the pentagon in the second plane are empty, and on some terraces none of these positions are occupied. Consider finally the outer components, the petals. These are usually decorated by Al only, but sometimes a mixture of Al + Mn appears. In short, the second-plane pentagon exhibits the highest chemical variation, and decorations at all sites are model-dependent.

Note that some sites have incomplete ten-atom decagons, which might appear in STM images as partial white flowers. One such feature is labeled WF′ in figure 6(a). The density of such features, compared to the full white flowers, is low. Therefore, in this analysis, we have excluded them.

3.3. Correlations with step heights

Two step heights are most commonly reported on the fivefold surface of i-Al–Pd–Mn: 0.41 and 0.66 nm [28, 39, 43–46]. On this surface, it has been reported that metal film morphologies [12, 23], and terrace widths [27], depend upon the height of the step adjoining the terrace. Because of such observations, there has been general speculation that step heights on quasicrystals may correspond to particular densities, compositions, or other features on the adjoining terraces [27]. Previously, we reported the first analysis showing that such a trend exists in the structural models, in the *long-range average* atomic density and chemical composition of the topmost surface plane of fivefold i-Al–Pd–Mn. Here, we show that trends also exist for the *local* features. We consider only the Pd− family of terminations, although it is fully expected that correlations could be found in the Pd+ family. The density of dark star sites predicted in the models is always significantly higher above the L-steps than above the M-steps. This is shown by the fourth column in table 5. This is true, not only for the average density of dark stars taken over all available terrace of a specified type, but also for the range of values of the density. Physically, this is because terraces above L-steps (see third column in table 5) correlates with a higher atomic density. This analysis is qualitatively consistent with the experimental data which, as noted in section 3.1, show that the density of dark stars changes from terrace to terrace [38–40].

4. Discussion

4.1. Variable chemical decorations

One main result of this paper is that, from the structural models, there are multiple chemical decorations of dark star and white flower atomic sites in the top layer of the fivefold surface of icosahedral Al–Pd–Mn. This can be true even within a single termination of a single model.

There have been several calculations of potential energy surfaces for chemisorbed species on quasicrystals and approximants [1, 13, 47–50]. All were limited in the sense that only one type of dark star decoration was considered. It is likely that chemisorption is influenced by the chemical nature of the second-plane pentagon. Hence, some dark star sites may be more inert than others, a factor that was not examined in the reported work.

This chemical variability could also be turned to advantage. In principle, studies of chemisorption could be used to test the validity of bulk structural models through the local chemical decorations of adsorption sites.

Table 5. Correlations between step heights (L or M), and densities of terminations and densities of pentagonal holes, in the Pd− family, for the four deterministic models. Heights of L- and M-type steps are 0.660 nm and 0.408 nm, respectively, for the fivefold surface of i-Al–Pd–Mn. In the four deterministic models, a layer is a pair of planes.

Model	Type of step bordering termination in down-going direction	Average atomic density in top plane of termination (nm^{-2})	Average density of Mackay-like pentagonal holes in the terminating layer (nm^{-2}). (Range of values is given in parentheses.) (Type is given in brackets.)
KG	L	6.6	0.405 (0.060–0.940) [A, B, C]
	M	8.9	0.025 (0.000–0.063) [A]
Boudard	L	6.8	0.431 (0.090–0.840) [A, B, C]
	M	8.8	0.010 (0.000–0.030) [A]
PK	L	6.9	0.405 (0.060–0.940) [A, B, C]
	M	8.8	0.016 (0.000–0.060) [A]
QG	L	6.8	0.428 (0.090–0.860) [A, B, C]
	M	8.8	0.015 (0.000–0.060) [A]

4.2. Different types of dark stars

Another new result of this paper is that STM resolves different types of dark stars, as shown in figures 3 and 4. The types, labeled A, B, and C, are distinguished by the number of complete pentagons surrounding the center (five, four, or less than 4, respectively). Incomplete pentagons typically contain a single protrusion near the center. The incomplete pentagons are predicted by the structural models, for cMs in the Pd− family. Another distinction is the different depths of the dark stars. The different depths could be due to atoms in the disordered dodecahedron in the cMs. They might also be due to the variable chemical decoration of the cut cluster, particularly the pentagon of atoms in the second plane (cf table 3).

There has been some controversy over whether the dark stars are cMs in the Pd− family, or cBs in the Pd+ family [21, 36, 51, 52]. Note that this debate also affects the white flower site, because the white flower is linked to the dark star by the nature of the family of terminating planes. Can the new STM observations resolve the debate? For cMs in the Pd− family, which have been the focus of this paper, the incomplete pentagons are due to the presence or absence of atoms, i.e. a structural variation. For cBs in the Pd+ family, our analysis (not presented here) shows that the incomplete pentagons would have to be attributed to chemical variations instead. The STM data can be interpreted more straightforwardly for cMs in the Pd− family, but the debate cannot be resolved conclusively from this observation alone. Stronger arguments for the Pd− family have been presented elsewhere [18], using average chemical compositions as well as gaps in the bulk structure between terminating planes.

4.3. Approach to analysis of bulk structure models

We find that many cMs in the Pd− family (and cBs in the Pd+ family) are imperfect, in the sense that the bulk cluster from which they originate has too few or too many atoms. Other authors have recognized that such imperfect clusters abound in the bulk models [33–35]. See section 2.2.

Our approach has been to identify local geometric arrangements of atoms in the top surface layer (top two planes) as cMs in the Pd− family, regardless of whether these atoms are part of a perfect cluster in the bulk. We believe that this approach is most appropriate for comparing the bulk models with STM images and with chemical properties.

This work has yielded several new insights. First, white flowers can be generated by intersections of the surface plane with a Mackay cluster at two different levels. This is analogous to the fact, also established in this paper, that dark stars can be generated by cuts at two different levels of the Mackay cluster (and that a single plane can contain both types of cuts). See figure 2. Second, certain atomic arrangements in the Pd− family are reasonable candidates for the white star and ring motifs seen in STM. Previously, it had been suggested that the ring motif might be specific to the Pd+ family [20, 36]. Finally, as an aside, we found that the Yamamoto model contains bulk Bergman and Mackay clusters, similar to the deterministic models.

4.4. Densities of dark stars

Figure 4 shows that the evaluation of dark star densities from STM images is affected by filtering, and it is probably best to analyze the raw, unfiltered images. However, another approach is available for determining densities. This is based on the fact that Ag islands nucleate at dark star sites. Counting Ag islands at low coverage, over many terraces, has yielded a density of 0.03–0.1 nm^{-2} [13, 15]. This range is incompatible with the total density of (A + B + C)-type cMs in the Pd− family, 0.26 nm^{-2}, shown in table 1. This suggests that dark stars are not all equally effective as nucleation sites for Ag islands. Their effectiveness may depend upon the presence of second-plane atoms in the disordered dodecahedron, or upon chemical variability in the atomic decorations of fixed sites.

The above analysis refers to the global, long-range average density of dark stars. However, there is a more local variation in the densities of dark stars—from terrace to terrace—both in experiment and in the models. In the models, the density of cMs correlates with the density of the topmost plane. See figure 7. Previously, we showed that the density of the top plane correlates with the height of the step adjoining the terrace, in the deterministic models [18]. Therefore, it follows that the density of cMs should correlate with the height of the step adjoining the terrace, and the present work confirms this trend. The dependence of terrace properties upon step height is a distinctive property of quasicrystal surfaces.

5. Conclusions

Compared with a typical surface of a single-crystal metal, there is a high degree of chemical heterogeneity in adsorption sites on the fivefold surface of i-Al–Pd–Mn. This can be true even within a single termination of a single model; the distribution broadens considerably when considering different terminations and different models. Hence, quasicrystal surfaces pose an unusual challenge for theoretical modeling.

Experimentally, different types of dark star sites can be resolved with STM, on the basis of the surrounding pentagons (consistent with the models) and also the depth of the hollow. The depth variation could result from the chemical decoration, or from the occupation of second-plane sites in the inner dodecahedron.

The global density of dark star sites, measured from the density of Ag islands which nucleate at those sites, is a factor of 2–9 lower than that predicted by the models. This suggests that dark star sites do not all have equal reactivity, consistent with their predicted variation in structural and chemical features. Locally, the density of dark stars in a given termination correlates with the height of the adjoining step and with the density of the topmost plane. This may explain why different properties have been reported for different terraces.

Acknowledgments

This work was supported by the Office of Science, Basic Energy Sciences, Materials Science Division of the US Department of Energy (USDOE). This manuscript has been authored by Iowa State University of Science and Technology under Contract No. DE–AC02–07CH11358 with the US Department of Energy. We are grateful to Denis Gratias, Marianne Quiquandon, Gerald Kasner, Zorka Papadopolos, Akiji Yamamoto, and Marc de Boissieu for supplying us with 3D atomic coordinates of the quasicrystal models. We are grateful to James W Evans for his careful reading and useful suggestions. We are thankful to Qisheng Lin for his help with the Diamond software which was used for plotting figure 2. We are thankful to Julian Ledieu for fruitful discussions.

References

[1] Ghosh C, Liu D-J, Schnitzenbaumer K J, Jenks C J, Thiel P A and Evans J W 2006 *Surf. Sci.* **600** 2220
[2] Cai T, Shi F, Shen Z, Gierer M, Goldman A I, Kramer M J, Jenks C J, Lograsso T A, Delaney D W, Thiel P A and Van Hove M A 2001 *Surf. Sci.* **495** 19
[3] Gierer M, Van Hove M A, Goldman A I, Shen Z, Chang S-L, Jenks C J, Zhang C-M and Thiel P A 1997 *Phys. Rev. Lett.* **78** 467
[4] Gierer M, Van Hove M A, Goldman A I, Shen Z, Chang S-L, Pinhero P J, Jenks C J, Anderegg J W, Zhang C-M and Thiel P A 1998 *Phys. Rev.* B **57** 7628
[5] Zheng J-C, Huan C H A, Wee A T S, Van Hove M A, Fadley C S, Shi F J, Rotenberg E, Barman S R, Paggel J J, Horn K, Ebert P and Urban K 2004 *Phys. Rev.* B **69** 134107
[6] Sharma H R, Shimoda M and Tsai A P 2007 *Adv. Phys.* **56** 403
[7] Shimoda M, Sharma H R and Tsai A P 2005 *Surf. Sci.* **598** 88
[8] Thiel P 2008 *Annu. Rev. Phys. Chem.* **59** 129
[9] Smerdon J A, Sharma H R, Ledieu J and McGrath R 2008 *J. Phys.: Condens. Matter* **20** 314005
[10] Ledieu J, Muryn C A, Thornton G, Diehl R D, Lograsso T A, Delaney D W and McGrath R 2001 *Surf. Sci.* **472** 89
[11] Cai T, Ledieu J, McGrath R, Fournée V, Lograsso T A, Ross A R and Thiel P A 2003 *Surf. Sci.* **526** 115
[12] Fournée V and Thiel P A 2005 *J. Phys. D: Appl. Phys.* **38** R83
[13] Unal B, Fournée V, Schnitzenbaumer K J, Ghosh C, Jenks C J, Ross A R, Lograsso T A, Evans J W and Thiel P A 2007 *Phys. Rev.* B **75** 064205
[14] Sharma H R, Shimoda M, Ross A R, Lograsso T A and Tsai A P 2005 *Phys. Rev.* B **72** 045428
[15] Fournée V, Cai T C, Ross A R, Lograsso T A, Evans J W and Thiel P A 2003 *Phys. Rev.* B **67** 033406
[16] Smerdon J A, Parle J K, Wearing L H, Lograsso T A, Ross A R and McGrath R 2008 *Phys. Rev.* B **78** 075407
[17] Ledieu J, Unsworth P, Lograsso T A, Ross A R and McGrath R 2006 *Phys. Rev.* B **73** 012204
[18] Unal B, Jenks C and Thiel P 2008 *Phys. Rev.* B **77** 195419
[19] Papadopolos Z, Pleasants P, Kasner G, Fournée V, Jenks C J, Ledieu J and McGrath R 2004 *Phys. Rev.* B **69** 224201
[20] Kasner G and Papadopolos Z 2006 *Phil. Mag.* **86** 813
[21] Krajci M, Hafner J, Ledieu J and McGrath R 2006 *Phys. Rev.* B **73** 024202
[22] Unal B, Evans J W, Lograsso T A, Ross A R, Jenks C J and Thiel P A 2007 *Phil. Mag.* **87** 2995
[23] Sharma H R, Shimoda M, Ross A R, Lograsso T A and Tsai A P 2006 *Phil. Mag.* **86** 807
[24] Barbier A, Le Floc'h D, Calvayrac Y and Gratias D 2002 *Phys. Rev. Lett.* **88** 085506
[25] Barbier L and Gratias D 2004 *Prog. Surf. Sci.* **75** 177
[26] Cai T, Fournée V, Lograsso T A, Ross A R and Thiel P A 2002 *Phys. Rev.* B **65** 140202
[27] Sharma H R, Fournée V, Shimoda M, Ross A R, Lograsso T A, Tsai A P and Yamamoto A 2004 *Phys. Rev. Lett.* **93** 165502
[28] Schaub T M, Bürgler D E, Güntherodt H-J and Suck J B 1994 *Phys. Rev. Lett.* **73** 1255
[29] Gratias D and Quiquandon M 2008 *Phil. Mag.* **88** 1887
[30] McGrath R, Leung L, Barrett S D and Ledieu J 2005 *Proc. R. Microsc. Soc.* **40** 215
[31] Bergman G 1957 *Acta Crystallogr.* **10** 254
[32] Mackay A L 1962 *Acta Crystallogr.* **15** 916
[33] Gratias D, Puyraimond F, Quiquandon M and Katz A 2000 *Phys. Rev.* B **63** 024202
[34] Quiquandon M and Gratias D 2006 *Phys. Rev.* B **74** 214205
[35] Loreto L, Farinato R, Catallo S, Janot C, Gerbasi G and De Angelis G 2003 *Physica* B **328** 193
[36] Papadopolos Z, Kasner G, Ledieu J, Cox E J, Richardson N V, Chen Q, Diehl R D, Lograsso T A, Ross A R and McGrath R 2002 *Phys. Rev.* B **66** 184207
[37] Yamamoto A, Takakura H and Tsai A P 2003 *Phys. Rev.* B **68** 094201
[38] Ledieu J and McGrath R 2003 *J. Phys.: Condens. Matter* **15** S3113
[39] Unal B, Lograsso T A, Ross A R, Jenks C J and Thiel P A 2005 *Phys. Rev.* B **71** 165411
[40] McGrath R, Ledieu J and Diehl R D 2004 *Prog. Surf. Sci.* **75** 131
[41] Krajci M and Hafner J 2005 *Phys. Rev.* B **71** 054202
[42] Ghosh C, Liu D J, Jenks C J, Thiel P A and Evans J W 2006 *Phil. Mag.* **86** 831
[43] Unal B, Lograsso T A, Ross A R, Jenks C J and Thiel P A 2006 *Phil. Mag.* **86** 819
[44] Barbier L, Le Floc'h D, Calvayrac Y and Gratias D 2002 *Phys. Rev. Lett.* **88** 085506
[45] Ledieu J, McGrath R, Diehl R D, Lograsso T A, Delaney D W, Papadopolos Z and Kasner G 2001 *Surf. Sci.* **492** L729
[46] Shen Z, Stoldt C R, Jenks C J, Lograsso T A and Thiel P A 1999 *Phys. Rev.* B **60** 14688
[47] Krajci M and Hafner J 2005 *Phys. Rev.* B **71** 184207
[48] Krajci M and Hafner J 2007 *Phil. Mag.* **87** 2981
[49] Krajci M and Hafner J 2008 *Surf. Sci.* **602** 182
[50] Krajci M and Hafner J 2008 *Phys. Rev.* B **77** 134202
[51] Papadopolos Z, Gröning O and Widmer R 2007 Clusters in F-phase iciosahedral quasicrystals *Models, Mysteries and Magic of Molecules* ed J C A Boeyens and J F Ogilvie (Berlin: Springer)
[52] Papadopolos Z, Widmer R and Groning O 2008 *Phil. Mag.* **88**